Applied Biochemistry and Biotechnology
https://doi.org/10.1007/s12010-022-04101-5

ORIGINAL ARTICLE

Practical and Rapid Membrane-Based Biosensor for Phenol Using Copper/Calcium-Enzyme Hybrid Nanoflowers

Felipe Pereira da Costa[1] · **Rosana Oliveira Henriques**[1] · **Agenor Furigo Junior**[1]

Accepted: 15 July 2022

Abstract
Phenol, a pollutant frequently found in chemical industries effluents, is highly toxic even in low concentrations. This study reports a green, simple, and rapid method for qualitative phenol biosensing using horseradish peroxidase (HRP) hybrid nanoflowers made with copper (Cu^{2+}-hNF) or calcium (Ca^{2+}-hNF) ions. The enzyme was immobilized through protein-inorganic self-assembly into hybrid structures and subsequently supported onto a polyvinylidene fluoride (PVDF) membrane. SEM, EDS, FTIR, and XRD techniques sustained the effective enzyme encapsulation into hybrid structures. The protein concentration in the structures was 0.25 $mg.mL^{-1}$ for both ions. The best temperature and pH were 60 °C and 7.4, respectively, for both hybrids and the free enzyme, suggesting that the immobilization did not affect the optimal conditions of the free HRP. Thermal stability from 25 to 70 °C and pH stability from 4.0 to 9.0 of the hybrids were also determined. Finally, using copper and calcium hybrids, both biosensors produced onto a PVDF membrane could detect phenol in concentrations ranging from 0.72 to 24.00 $\mu mol.mL^{-1}$ in 1 min. In contrast, control biosensors produced with free enzyme have not presented a visible color change in the same conditions. The findings suggest a promising application of the developed biosensors in functional phenol detection.

Keywords Organic–inorganic hybrids · Hybrid nanoflowers · Enzyme immobilization

Introduction

Peroxidases (EC 1.11.1.x) encompass a vast group of valuable biocatalysts involved in the numerous oxidative reactions which use hydrogen peroxide as electron acceptors. They perform an essential function in many biologic reactions in almost all living organisms. Consequently, it is not difficult to find peroxidases with distinct origins being employed in the most diverse scenarios, such as food engineering [1–3], pharmaceutical applications [4, 5], and wastewater treatment [6–10]. Among those, horseradish peroxidase (HRP) represents the principal source of commercial peroxidases [11].

✉ Rosana Oliveira Henriques
rosana.henriques@posgrad.ufsc.br

[1] Department of Chemical and Food Engineering, Federal University of Santa Catarina - UFSC, CEP, Florianópolis, SC 88040-900, Brazil

Despite all sources of peroxidases and the relative facility to obtain them, enzyme immobilization is needed to ensure superior stability, facilitated recovery, and consequent re-usability [12]. However, traditional immobilization techniques tend to cause a decrease in enzyme activity, which might represent additional costs to the process. Against this background, organic–inorganic hybrid nanoflowers are a recent and facile immobilization approach that enables improved stability and higher activities in immobilized enzymes compared to their free form [13]. Since the first report of their synthesis, organic–inorganic hybrids have been broadly employed in diverse applications, like bioremediation [13–17] and synthetic chemicals production [18–20]. Nevertheless, the main application of hybrid nanoflowers has been in biosensors development [21–26].

Enzymatic biosensors have been widely used to detect phenol due to their high toxicity and recurrent incidence in effluents of many chemical industries, such as paper and cellulose, petroleum refining, pharmaceutical, and metal coating [27, 28]. Different enzymes are employed for this purpose, like tyrosinase [29–34], laccase [35–39], and peroxidase [40–46]. However, those biosensors often exploit interwoven elaborated techniques, which might portray a barrier to in situ phenol analysis as an environmental pollutant.

Hence, the present study aimed to develop a simple, rapid, and low-cost qualitative biosensor for phenol employing copper-HRP and calcium-HRP hybrid nanoflowers. The biosensors produced were tested for different phenol concentrations to determine their detection limit. The influence of protein concentration and the metal ion in nanoflowers synthesis was examined. Furthermore, the prepared hybrids were characterized by scanning electron microscopy (SEM), energy-dispersive X-ray spectroscopy (EDS), Fourier transform infrared spectroscopy (FTIR), and powdered X-ray diffraction (XRD). Additionally, kinetic parameters for both hybrids were also established.

Methodology

Chemicals and Materials

Horseradish peroxidase (HRP) was obtained from Toyobo (Brazil). 4-aminoantypirine, H_2O_2 (35%), Na_2HPO_4, NaH_2PO_4, NaCl, $CaCl_2$, and $CuSO_4$ of analytical grade were employed in the assays. PVDF Hydrophilic Membrane (GVS, USA) with a pore diameter of 0.22 μm was used to produce the biosensors. Distilled water was used in all experiments.

Preparation of Copper-HRP and Calcium–HRP Nanoflowers

The copper-HRP hybrid nanoflowers (Cu^{2+}-hNF) were synthesized following previously reported methods [13, 42, 47–50] with some modifications. In a typical experiment, 67 μL of $CuSO_4$ (120 mM) were added to 10 mL of phosphate-buffered saline (PBS) (100 mM, pH 7.4) with 0.1% NaCl (w/w) containing HRP in different concentrations from 0.1 to 1.0 $mg.mL^{-1}$. This mixture was stirred with a vortex for 30 s and then incubated at 4 °C for 72 h. The precipitated with the hybrids was collected through centrifugation at 4000 rpm for 15 min. Calcium-HRP hybrid nanoflowers (Ca^{2+}-hNF) were synthesized with the same procedure, using the best enzyme concentration from Cu^{2+}-hNF experiments and 67 μL of $CaCl_2$ (120 mM) as the donor of calcium ions.

Characterization of Copper-HRP and Calcium–HRP Hybrid Nanoflowers

The morphology of Cu^{2+}-hNF and Ca^{2+}-hNF was analyzed by scanning electron microscopy (SEM, JEOL JSM-6390LV). The electron microscope was equipped with energy-dispersive X-ray spectroscopy (EDS) to determine the elemental composition of the structures as well. Samples were prepared by dripping 10 µL of the hNFs suspension onto polyvinylidene fluoride (PVDF) membranes with 0.22 µm of pore size, which were dried in a desiccator at room temperature for 24 h. Functional groups present in the hybrids and the free enzyme were identified and characterized by Fourier transform infrared spectroscopy (FTIR, AGILENT TECHNOLOGIES – Cary 660) from 400 to 4000 cm^{-1}. Powdered X-ray diffraction (XRD, Enraf – Nonius, model Cade – 4) technique within the 2θ range from 5 to 60° was used to identify the crystal structure of HRP hybrid nanoflowers.

Enzyme Activity Assays

The peroxidase activity was determined using a method previously proposed by Trinder (1969) with modifications. This approach employs 4-aminoantipyrine (4-AAP) as a hydrogen donor and is measured spectrophotometrically by the hydrogen peroxide degradation and consequent formation of quinoneimine, a pinkish antipyrine dye [51, 52]. This reaction is represented in Fig. 1:

For the assay at 25 °C, 1.5 mL of 0.0017 M hydrogen peroxide (in PBS 0.2 M, pH 7.4) was mixed with 1.4 mL of a solution containing 0.0025 M 4-AAP and 0.17 M phenol. The reaction was started by adding 0.1 mL of free HRP 0.25 $mg.mL^{-1}$, Cu^{2+}-hNF 1.0 $mg.mL^{-1}$, or Ca^{2+}-hNF 0.5 $mg.mL^{-1}$ suspension to the reaction medium. The absorbance was measured after 1 min in 510 nm by spectrophotometry (Hitachi, model U–2900). In this work, one HRP activity unit (U) was defined as the amount of enzyme that produces 1 mmol of quinoneimine per minute under experimental conditions. Enzymatic activity of free enzyme and hNFs was calculated with the Eq. 1 [52]:

$$A = \frac{\Delta Abs_{510}}{\varepsilon \times b \times t} \tag{1}$$

where A is the enzymatic activity of HRP ($U.L^{-1}$), ΔAbs_{510} is the absorbance variance at 510 nm, ε is the molar absorption coefficient of quinoneimine dye (6.58 $L.mmol^{-1}.cm^{-1}$), b is the light path length (1 cm), and t is the reaction time (1 min).

Encapsulation Yield

The encapsulation yield (Y) determines the percentage of the initial free enzyme reduced to the immobilized form. The enzymatic activities of the free HRP and the hybrid

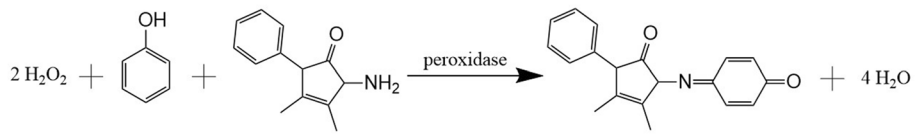

Fig. 1 Scheme of the peroxidase-catalyzed reaction of H_2O_2, phenol, and 4-AAP

nanoflowers were carried out as described previously in the "Enzyme Activity Assays" section. Subsequently, the immobilization yield was calculated using Eq. 2:

$$Y(\%) = 100 \times \left(\frac{A_i - A_s}{A_i} \right) \tag{2}$$

where A_i is the initial activity in the HRP solution and A_s is the activity of the supernatant obtained by centrifugation of the reaction medium after the hybrid nanoflowers synthesis.

pH and Temperature Effect on the Enzyme Activities of the Free HRP and hNFs Preparations

Different buffers, such as McIlvaine buffer 0.1 M for pH 3.0, 4.0, and 5.0; phosphate buffer 0.1 M for pH 6.0, 7.0, and 7.4; Tris–HCl buffer 0.1 M for pH 8.0 and 9.0; Sorensen's glycine buffer for pH 10.0, 11.0, and 12.0; and NaOH 0.1 M for pH 13.0, were used to produce 0.0017 M hydrogen peroxide solution to evaluate pH influence on the enzyme activity. The activity assays were carried out using the phenol and 4-AAP methods previously described.

The reagents and enzymatic preparations were incubated for 5 min in a thermostatic bath (SolidSteel, Model SSDc – 10 L) at several temperatures (from 25 to 70 °C) before the reaction started. As stated above, the whole reaction was carried out within a pH 7.4 buffer at the intended temperature. Both pH and temperature-dependent activities were expressed as relative activities (%), where the higher value for each sample was set as 100%. Error bars represent the standard deviation of three independent experiments.

Effect of the pH and Temperature on the Stability of the Free HRP and hNFs Preparations

To assess the pH influence on the stability of free and immobilized preparations, all hNFs produced in a typical synthesis, as well as the equivalent amount of HRP, were suspended in 2.0 mL of various buffer solutions: citrate buffer 0.1 M for pH 4.0 and 5.0; phosphate buffer for pH 6.0 and 7.4; and Tris–HCl buffer 0.1 M for pH 8.0 and 9.0. The activities were measured using 0.1 mL of the enzyme or hNFs preparations in the intended pH, following the identical procedure described in the "Enzyme Activity Assays" section at different times, from 0 to 8 h.

The thermal stability of the free enzyme and hNFs was appraised in the following way: first, all hNFs synthesized in a typical experiment were suspended in 2.0 mL of PBS 0.1 M, pH 7.4. A solution of an equivalent amount of the free enzyme was made the same way. Then, these preparations were placed in a thermostatic bath at settled temperatures of 50, 60, and 70 °C. Finally, 0.1 mL was taken from each sample at different times (0, 2, 4, 6, and 8 h), and activity was measured at room temperature, following the phenol method previously described. The stability was estimated by the relative activity (%) in the function of the time, considering the initial activity as 100%.

Determination of the Kinetic Parameters KM, V_{max}, and k_{cat}

Initial specific reaction rates (V_0) were obtained by measuring the absorbance variation at 25 °C, 510 nm, and 1 min of reaction time. The reaction medium was prepared mixing

0.1 mL of enzyme sample (HRP 0.25 mg.mL^{-1}, Cu^{2+}-hNF 1.0 mg.mL^{-1}, or Ca^{2+}-hNF 0.5 mg.mL^{-1}), 1.5 mL of 0.0017 M hydrogen peroxide in PBS 0.2 M and pH 7.4, 0.7 mL of 0.005 M 4-AAP, and 0.7 mL of phenol in different concentrations, from 3 to 400 mM. V_0 values were calculated with Eq. 3:

$$V_0 = \frac{\Delta Abs_{510}}{\varepsilon \times b \times t \times C_E} \tag{3}$$

where V_0 is the initial specific reaction rate (μmol.min^{-1}.mg^{-1}), ΔAbs_{510} is the absorbance variance at 510 nm, ε is the molar absorption coefficient of quinoneimine dye (6.58 L.mmol^{-1}.cm^{-1}), b is the light path length (1 cm), t is the reaction time (1 min), and C_E is the enzyme concentration in the assay (mg.mL^{-1}). Results are presented as average result ± standard deviation, estimated from the Lineweaver–Burk graph, plotted in Sigmaplot 14.0, using GNU Octave 6.2.0 software.

Kinetic parameters K_M (μmol.mL^{-1}) and V_{max} (μmol.min^{-1}.mg^{-1}) of the Michaelis–Menten model for simple enzymatic reactions (Eq. 4) were then determined for the free enzyme and both hybrids, using phenol as the substrate.

$$V_0 = \frac{V_{max}[S]}{K_M + [S]} \tag{4}$$

where V_0 is the initial specific reaction rate (μmol.min^{-1}.mg^{-1}), V_{max} is the maximum specific reaction rate (μmol.min^{-1}.mg^{-1}), K_M is the Michaelis constant (μmol.mL^{-1}), and $[S]$ is the substrate concentration (μmol.mL^{-1}).

Subsequently, the turnover number, or k_{cat}, was also determined. Values were obtained by using Eq. 5:

$$k_{cat} = V_{max} M_{HRP} \tag{5}$$

where k_{cat} is the turnover number (min^{-1}), V_{max} is the maximum specific reaction rate (μmol.min^{-1}.mg^{-1}), and M_{HRP} is the molar weight of the HRP enzyme (44.0 mg.μmol^{-1}).

Membrane-Based Phenol Detection Using HRP–Copper, and HRP–Calcium Hybrid Nanoflowers

A qualitative membrane-based biosensor was developed employing a craft-cutting technique to provide a cost-efficient phenol detector. First, 1 cm^2 square was cut from a PVDF membrane, with 0.22 μm of pore size, and 10 μL of Cu^{2+}-hNF or Ca^{2+}-hNF 1.0 mg.mL^{-1} suspensions were dripped onto the squares and left to dry in a desiccator at room temperature for 12 h. For comparison purposes, control biosensors were made with 10 μL of an equivalent amount of the free enzyme. Subsequently, the efficacy of the biosensors for phenol detection was investigated with 50 μL of a sample solution. This solution contained H_2O_2 0.88 μmol.mL^{-1}, 4-AAP 1.1 μmol.mL^{-1}, and phenol in different concentrations from 0.72 to 24.00 μmol.mL^{-1} in PBS 0.2 M with pH 7.4, which was dripped onto the biosensors. As a result, a pink color appears on the hNFs membranes to prove the presence of phenol.

Results and Discussion

Synthesis and Characterization of Cu^{2+}-hNF and Ca^{2+}-hNF

As a recent and promising enzyme immobilization technique, organic–inorganic hybrid nanoflowers are micro-sized structures that present nanoscale patterns and exhibit flower-like shapes [50]. The growth mechanism of these nanoflowers has been widely described [13, 42, 53–55]. Briefly, three steps summarize the mechanism: nucleation, growth, and compilation [47, 56]. First, amide groups present in the enzyme backbone complex with metal ions, while the same ions react with $(PO_4)^{3-}$ from PBS to form primary crystals of $Cu_3(PO_4)_2 \bullet 3H_2O$ or $CaHPO_4$ and $Ca_3(PO_4)_2 \bullet 2H_2O$ embedded with HRP. These complexes act as nucleation points for hybrid nanoflowers assembly; therefore, they depend on the enzyme in the synthesis medium. It has been shown that lower enzyme concentrations lead to fewer nucleation points and, consequently, hybrids with a greater diameter [57, 58]. The growth stage, which occurs anisotropically, is marked by the continuous addition of enzyme molecules to those primary crystals, creating the first hybrid petals. Then, the compilation stage is observed, where the enzyme induces the metal-phosphate crystallization into a basis for new petals and simultaneously attaches petals in flower-like structures [47].

The effect of the initial concentration of HRP in the morphology of Cu^{2+}-hNF was investigated by SEM analysis (Fig. 2). With 0.10 $mg_{HRP}.mL^{-1}$, hybrid structures (Fig. 2A) showed loose petals, although they had adequate size and formation. Higher concentrations

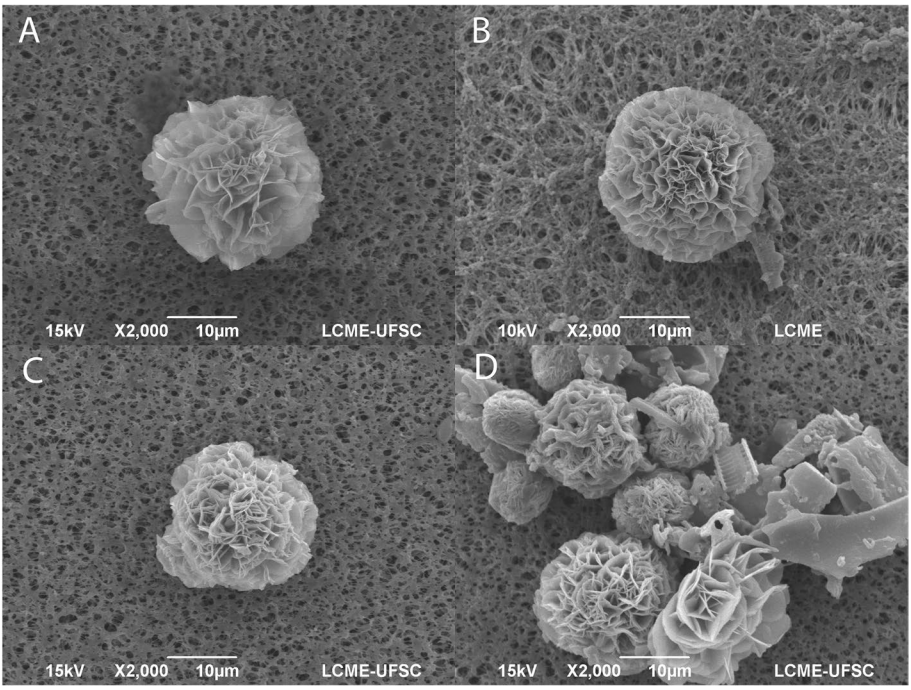

Fig. 2 SEM images of Cu^{2+}-hNF produced with different initial HRP concentration of (A) 0.10 $mg.mL^{-1}$, (B) 0.25 $mg.mL^{-1}$, (C) 0.50 $mg.mL^{-1}$, and (D) 1.00 $mg.mL^{-1}$, at 4 °C for 72 h

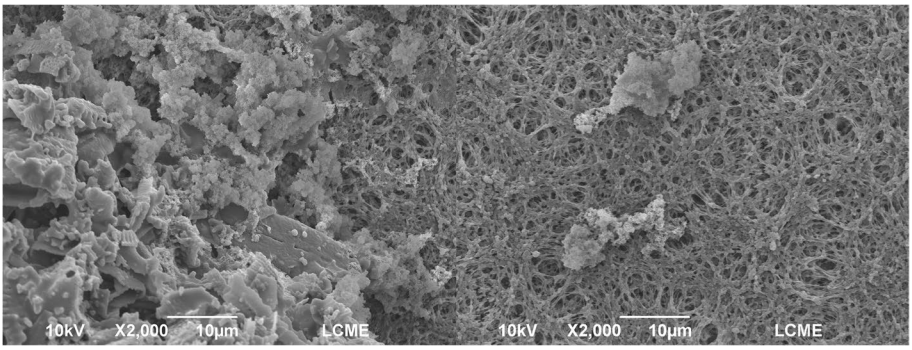

Fig. 3 SEM images of Ca^{2+}-hNF produced with an initial concentration of HRP of 0.25 $mg.mL^{-1}$, at 4 °C for 72 h

of 0.25, 0.50, and 1.00 $mg_{HRP}.mL^{-1}$ had led to tightened petals and consequent greater ratio surface area per volume (Fig. 2B, C and D). It is noticeable that Cu^{2+}-hNF was produced with 0.25 $mg_{HRP}.mL^{-1}$ exhibited greater spherical shape consistency and distinct petal-like structures.

Ca^{2+}-hNF was synthesized using the initial HRP concentration of 0.25 $mg_{HRP}.mL^{-1}$ and the same ion concentration of 80 mM, according to good structure formation seen in SEM results of Cu^{2+}-hNF. SEM images of these new hybrids are shown in Fig. 3. The SEM for free HRP is shown in Fig. 4, and it is possible to see that any structures were presented.

Nevertheless, the flower-like structure was not well determined in this case. The difference between the calcium and copper hybrid produced under the same conditions might be explained by the formation of contrasting metal-phosphates structures, mainly amorphous for calcium and crystalline for copper [59]. Ke et al. (2016) have shown in their study with lipase-calcium hybrids that the flower-like structure only appeared with the specific PBS concentration of 20 mM. At lower concentrations, there was no complete formation of the petals. In comparison, an excess of calcium phosphate was added to these petals at higher concentrations, and nanoflowers were not seen in either case [60]. ZHANG et al. (2020) have proved that the calcium ion concentration also influences the hybrid's morphologies.

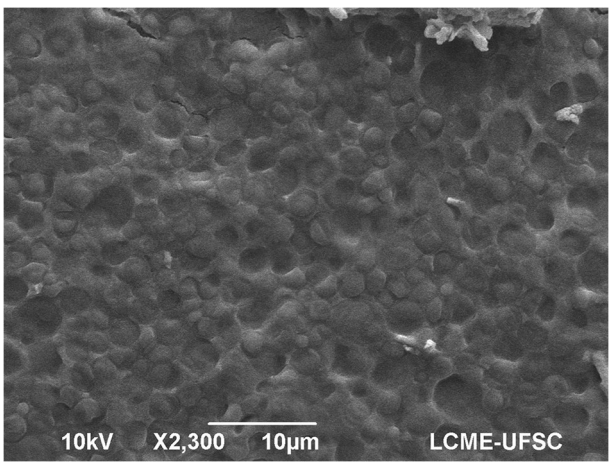

Fig. 4 SEM images from the free HRP

Table 1 Encapsulation yield of HRP based on residual enzyme activity in the supernatant

Metal	Initial enzyme concentration (mg. mL^{-1})	Encapsulation yield (%)
Cu^{2+}	0.10	85.7 ± 0.7
	0.25	92.3 ± 0.2
	0.50	89.2 ± 1.1
Ca^{2+}	0.10	83.5 ± 0.6
	0.25	92.0 ± 0.7
	0.50	89.4 ± 0.3

Their work about lipase-inorganic nanoflowers reported that flower-like structures were only observed when calcium ion concentrations higher than 200 mM were used. Below this point, irregular nanoparticles were formed [19]. Furthermore, Yu and co-workers (2018) have also reported that calcium-organic hybrids did not present the same evident shape that copper nanoflowers usually do with neither of the six enzymes tested, even though each had a distinct appearance [59].

Sheldon and van Pelt (2013) described that the immobilization yield could be precisely established by measuring the residual activity in the enzyme solution after the immobilization process and comparing this to the initial activity [12]. Different initial enzyme concentrations were tested in hNFs synthesis. The average results of encapsulation yield and respective experimental standard deviations of three independent experiments are shown in Table 1. These results suggest an optimal initial enzyme concentration of 0.25 mg.mL^{-1} for both metal ions, leading to a higher encapsulation yield. The higher encapsulation yields were 92.3% and 92.0% for Cu^{2+}-hNF and Ca^{2+}-hNF, respectively. With an enzyme concentration of 0.10 mg.mL^{-1}, this encapsulation yield decreased to 85.7% in Cu^{2+}-hNF and 83.5% in Ca^{2+}-hNF. Likewise, this value was also reduced with an initial HRP of 0.50 mg.mL^{-1} to 89.2% in Cu^{2+}-hNF and 89.4% in Ca^{2+}-hNF. According to this outcome and those published in prior works [22, 48, 61–63], it is possible to deduce an optimal protein concentration that leads to the highest encapsulation yield value. Based on morphologies features observed in Cu^{2+}-hNF and on protein embedding efficiency for both hybrids, the initial protein concentration of 0.25 mg.mL^{-1} was fixed for all subsequent characterization and application.

The EDS technique revealed the elemental composition of hybrid nanoflowers. The EDS spectrum results in atom percentage are found in Table 2. Characteristic peaks of classical elements such as C, O, and P commonly reported were observed in both hybrids [19, 48, 64, 65]. Copper was verified in an atom amount of 16.30% in Cu^{2+}-hNF, and the atom

Table 2 Elemental composition of hybrid nanoflowers

Element	*Cu^{2+}-hNF* (atom %)	*Ca^{2+}-hNF* (atom %)
C-K	25.19	8.16
O-K	29.80	47.29
P-K	18.17	11.21
Cl-K	4.65	0.31
Cu-K	16.30	–
Ca-K	–	27.97

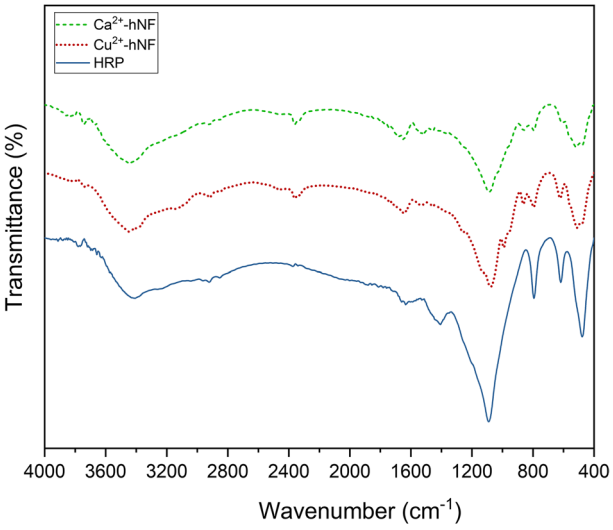

Fig. 5 FTIR of Ca^{2+}-hNF, Cu^{2+}-hNF and free HRP

concentration of calcium in Ca^{2+}-hNF was 27.97%, proving the formation of organic–inorganic structures. Chlorine was also recognized in EDS analysis for both hybrids but more expressively in copper ones. These ions, obtained by NaCl in solution, perform an essential role in hNFs formation [53, 55, 66]. It was first described by Sun et al. (2014) when the authors noted that no nanoflowers were formed without chloride ions [53]. The statement was supported by Somtkurk et al. (2016), who had produced a blue precipitate with no typical nanoflower-like shape when there was no Cl^- in reaction bulk, and by Ariza-Avidad and co-workers (2016), who have also found chlorine atoms in hNFs by EDS analysis [55, 66].

FTIR analysis was carried out to identify chemical structures and prove organic–inorganic hybrid nanoflowers' formation. The spectroscopy results are shown in Fig. 5. Characteristic bending vibrations of O═P─O were observed in ~ 560 cm^{-1}, and ~ 630 cm^{-1} in both hybrids might be attributed to metal-phosphate groups in the structures [55, 67]. The stretching bands 1400–1630 were attributed to NH_2 groups from peptide bonds [68]. Considerable peak weakening in 1020–1220 cm^{-1} and 1350–1470 cm^{-1} bands suggests changes in the secondary structure of the enzyme in the hybrid's formation [60]. The peaks at 2800–3000 cm^{-1} are typical for CH_2 and CH_3 groups, while OH and NH groups stretching bands are found at ~ 3450 cm^{-1} [55, 66]. Another significant absorption band, noticed in ~ 1090 cm^{-1}, might refer to the asymmetric vibration of Si–O [69].

This result is consistent with silica structures, observed in SEM analysis and characterized by EDS in all samples tested. SEM images of those structures are presented in Fig. 6. Although the stabilizers used in the commercial enzyme are not specified, we believed that silica compounds were present in the free enzyme sample for this purpose. Additionally, even in the presence of silica compounds, the hybrid synthesis was not affected.

XRD technique was employed to characterize the crystal phases of both hybrids, as presented in Fig. 7. XRD analysis has shown that copper hybrids (Fig. 7A) have peak consistency with $Cu_3(PO_4)_2 \bullet 3H_2O$ crystals pattern (JCPDS No. 00–022-0548). This result is coherent with the previously reported synthesis of copper-enzyme hybrids [58, 70–72]. Likewise, XRD of calcium hybrids (Fig. 7B) has exhibited correspondence with $Ca_3(PO_4)_2 \bullet 2H_2O$ (JCPDS No. 18–0303) and $CaHPO_4$ (JCPDS No. 9–80), both already communicated in earlier research of calcium-enzyme structures [19, 54].

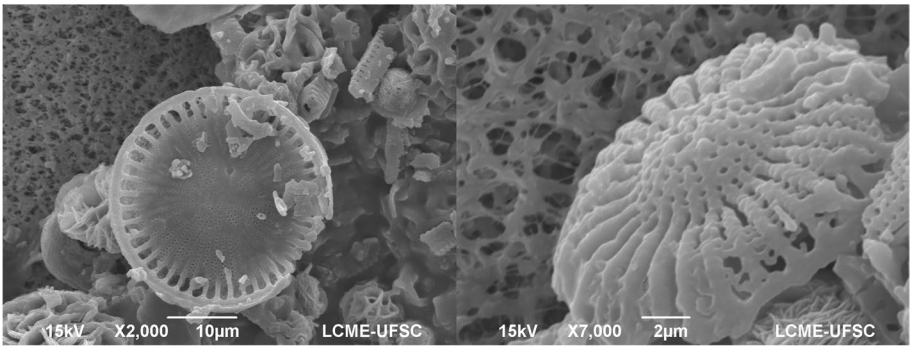

Fig. 6 SEM images of silica structures

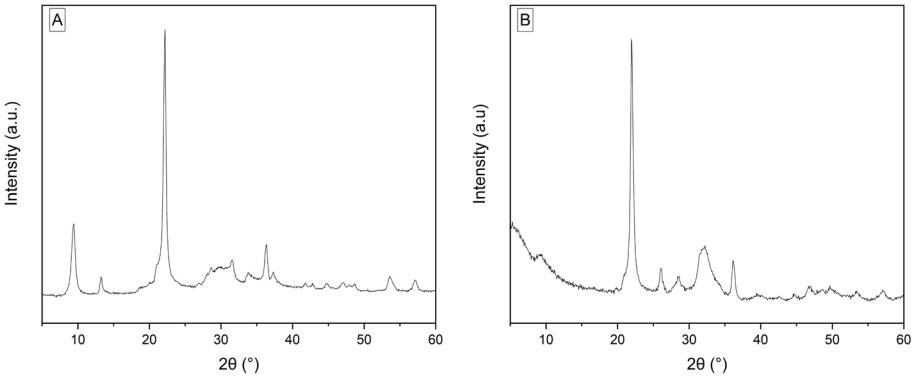

Fig. 7 XRD spectrum of (A) Cu^{2+}-hNF and (B) Ca^{2+}-hNF

It was also possible to visualize a major peak in both structures at $2\theta \approx 22°$, referring to SiO_2 crystals (JCPDS No. 46–1045). This outcome confirms the presence of the structures seen in the preceding analysis carried out in this work.

pH and Temperature Effect on the Enzyme Activities of the free HRP and hNFs Preparations

Activity assays determined the optimal conditions of use for free HRP and hNFs. First, experiments to obtain the best pH were carried out at different pH values at room temperature. The results are reported in Fig. 9 as relative activity. The highest activity for each biocatalyst was set as 100%, and other points were calculated as a fraction of this value. The optimal pH was 7.4, independently of the biocatalyst used. It shows that the hybrid formation of HRP with copper and calcium phosphates did not affect the enzyme's best pH value. Similar behavior was detected by Rong et al. (2017) and by Memon et al. (2019), where copper-enzyme and calcium-enzyme hybrids, respectively, presented the same best pH value that the free studied enzymes [16, 54].

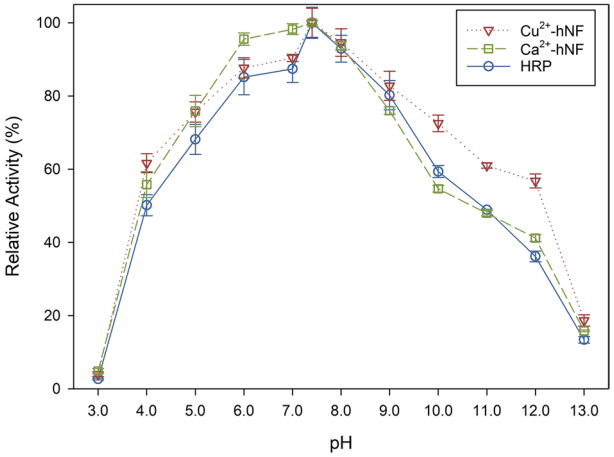

Fig. 8 Relative activity as a function of pH at 25 °C for Cu^{2+}-hNF, Ca^{2+}-hNF, and free HRP

However, it is possible to notice that Cu^{2+}-hNF presents less activity loss with a pH increase from 9.0 to 12.0 than free HRP and Ca^{2+}-hNF. Previous works have also reported similar behavior in higher pH values for copper-enzyme hybrids than the free enzyme, suggesting greater enzyme stability within the tested conditions [48, 73].

Subsequently, using the best pH value, activity was tested at different temperatures from 25 to 70 °C. The relative activity as a function of the highest activity for each biocatalyst is in Figs 8, and 9. As it happened with pH evaluation, the synthesis of Cu^{2+}-hNFs and Ca^{2+}-hNFs did not affect the optimal temperature, which was detected to be 60 °C for all cases, as expected according to literature data [18, 53].

Effect of pH and Temperature on the Stability of the Free HRP and hNFs Preparations

The effect of pH and temperature on the stability of the free enzyme and hybrid preparations was also investigated. All the results are expressed as relative activity, where the initial activity for each biocatalyst was set as 100%.

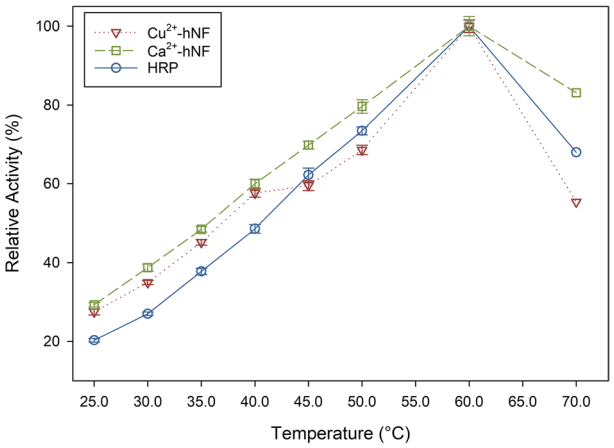

Fig. 9 Relative activity as a function of temperature in pH 7.4 for Cu^{2+}-hNF, Ca^{2+}-hNF, and free HRP

According to the pH stability analysis, in pH of 6.0 to 8.0 (Fig. 10C, D, and E), free enzyme and hybrid preparations with copper and calcium showed similar deactivation profiles. Consequently, enzyme immobilization did not significantly affect the enzyme stability in those pH values. On the other hand, in pH of 9.0 (Fig. 10F), both hybrids presented discrete superior stability to the free form. In fact, after 24 h, copper and calcium hybrids maintained 97.97% and 96.38% of their initial activities, while free HRP kept 92.82%. The smallest activity losses in 24 h of 5.51%, 6.49%, and 4.07% (free HRP, Cu^{2+}-hNF, and Ca^{2+}-hNF, respectively) were observed at the optimal pH of 7.4.

However, calcium hybrids exhibited more significant deactivation in acid mediums than copper and free enzymes (Figs. 10A and B). This outcome suggests that hybrids' stability is completely related to organic and inorganic constituents. In this sense, conjugated polyketone reductase-calcium phosphate hybrids with sodium alginate coating prepared by

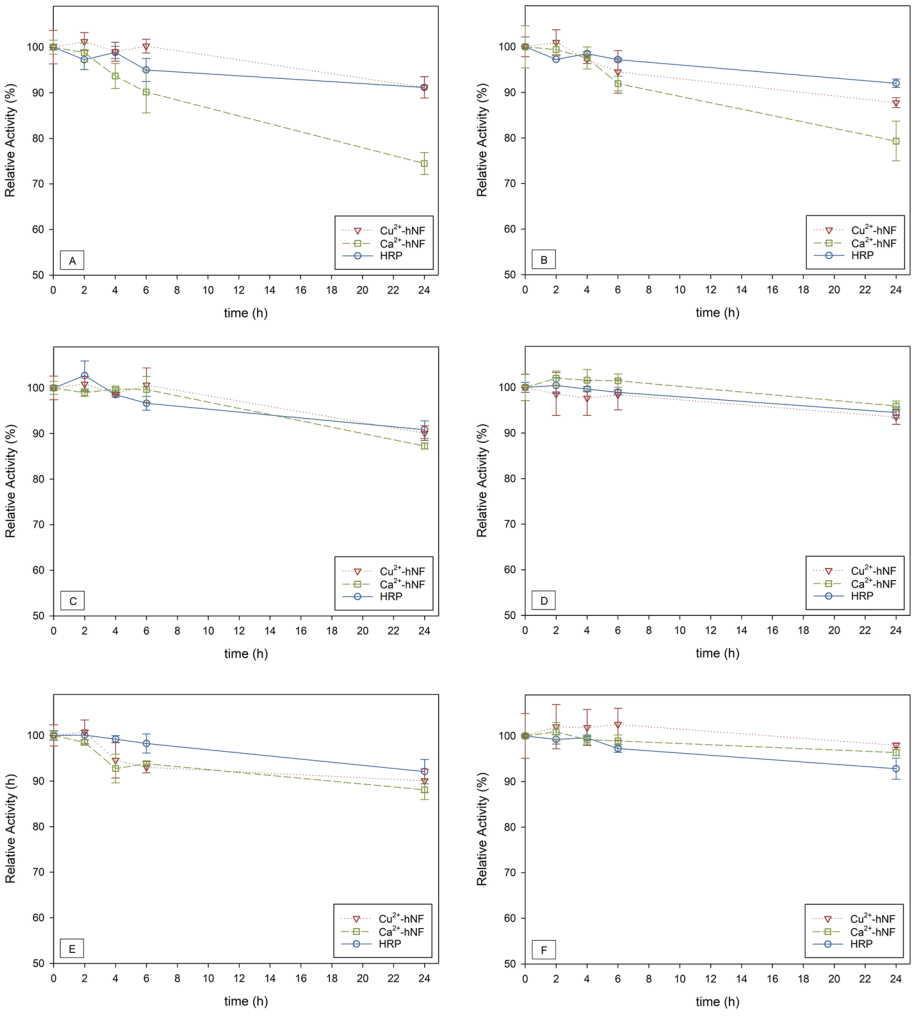

Fig. 10 Enzyme stability for Cu^{2+}-hNF, Ca^{2+}-hNF and free HRP in pH (A) 4.0, (B) 5.0, (C) 6.0, (D) 7.4, (E) 8.0, and (F) 9.0, at 25 °C

Cheng et al. (2020) presented a notably smaller residual activity in acid mediums than free enzymes [74]. Consistently, Chen et al. (2018) have shown that, despite the higher activity of calcium-enzyme hybrids, the immobilized form of aldo–keto reductase (AKR) with calcium phosphate was more sensitive to acid pH changes than free enzyme [75]. In the same study, the authors have also noted that alcohol dehydrogenase (ADH) hybrids could keep the activity in the function of pH variance more easily, confirming the dependence of hybrid composition on their activity [75].

Thermal stability analysis indicated excellent stability for both hybrids and the free enzyme at 50 °C (Fig. 11A), where no considerable activity loss after 8 h. At 60 °C (Fig. 11B), the optimal temperature for the enzyme activity and the residual activity after 8 h were 79.61%, 76.61%, and 74.97% for free HRP, copper, and calcium hybrids, respectively. Finally, at 70 °C (Fig. 11C), the favorable effect of the enzyme immobilization in copper hybrids in the stability is notable. While the free enzyme lost all its activity in 6 h, copper hybrids showed only 5.59% of residual activity, and calcium preparations maintained 26.42% in 8 h. This result suggests the greater stability of HRP-calcium hybrids in higher temperatures. Analogously, Duan, Li, and Zhang (2018) have noted that metal-enzyme hybrids had greater thermal stability than free enzymes. Still, also calcium-enzyme tended to show the smallest activity loss in all temperature ranges, from 30 to 80 °C [76]. Chen and co-workers (2018) also presented improved thermal stabilities in calcium phosphate-enzyme hybrids in 8 h in temperatures from 30 to 60 °C for both enzymes ADH and AKR. However, this stability upgrade was much more significant in AKR hybrids [75].

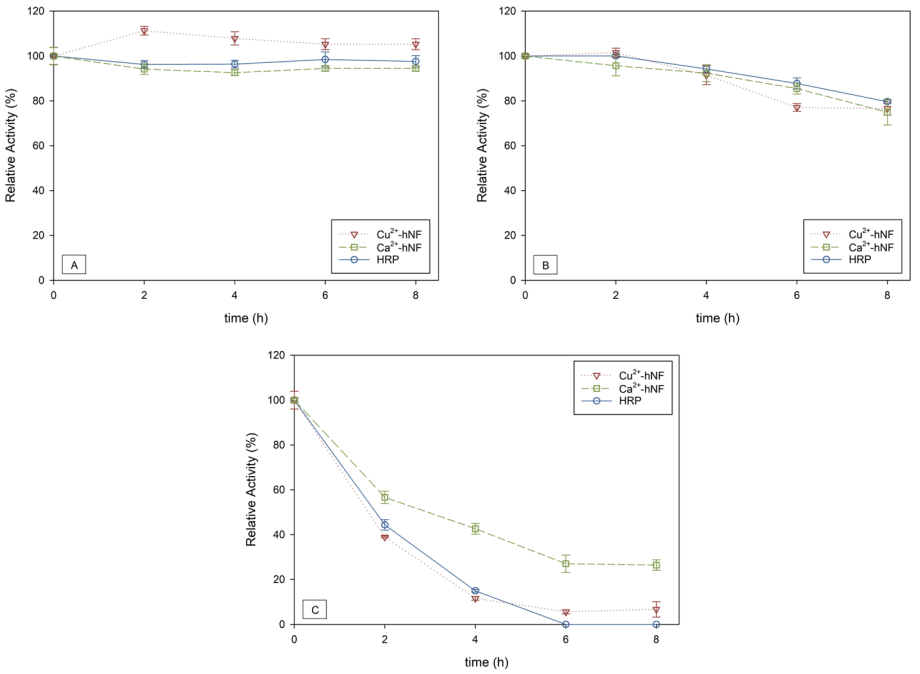

Fig. 11 Enzyme thermal stability for Cu^{2+}-hNF, Ca^{2+}-hNF, and free HRP in (A) 50 °C, (B) 60 °C, and (C) 70 °C, in pH 7.4

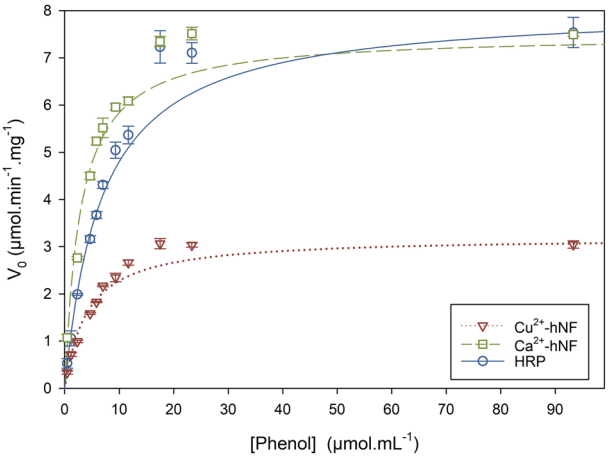

Fig. 12 Initial specific reaction rates as a function function of phenol concentration for Cu^{2+}-hNF, Ca^{2+}-hNF, and free HRP, in pH 7.4 at 25 °C

Michaelis–Menten Kinetic Parameters

A 10-step mechanism of the co-oxidation of phenols and 4-AAP, which includes quinonimine production, was proposed by Metelitza, Litvinchuk, and Savenkova (1991) [77]. However, even though the reaction has a complex mechanism, the initial reaction rate, as shown in Fig 12, is a function of phenol concentration. This result suggests that, in the tested conditions, phenol consumption is the slow step of the mechanism, and it determines, consequently, the reaction rate. Although HRP immobilization into Ca^{2+}-hNF did not lead to a considerable change in the kinetic profile of phenol consumption, Cu^{2+}-hNF seems to have had a substantial decrease in the maximum initial specific reaction rate.

A double reciprocal plot, which can be visualized in Fig. 13, was finally produced to determine the kinetic parameters K_M, V_{max}, and k_{cat} (Table 3) and to quantify those differences after immobilization. Excellent model fitting to the experimental data, evidenced by parameter R^2 equal to 0.994, 0.995, and 0.990 for free-HRP, copper, and calcium hybrids, respectively, indicates the validity of the method approximation.

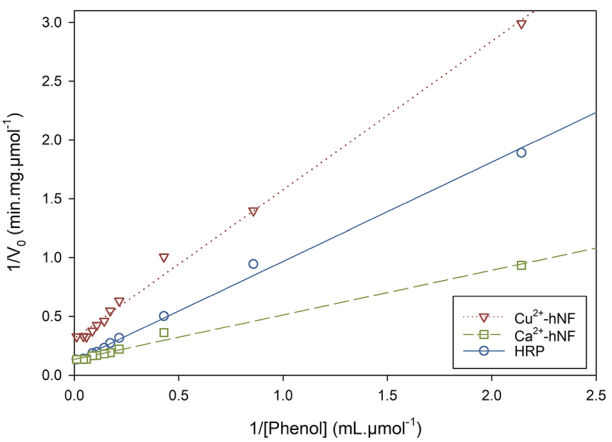

Fig. 13 Lineweaver–Burk plot for Cu^{2+}-hNF, Ca^{2+}-hNF, and free HRP

Table 3 Kinetic parameters of Cu^{2+}-hNF, Ca^{2+}-hNF and free HRP

Biocatalyst form	K_M (μmol.mL^{-1})	V_{max} (μmol. min^{-1}.mg^{-1})	k_{cat} (s^{-1})	k_{cat}/K_M (s^{-1}.mM^{-1})
free-HRP	6.82 ± 0.87	8.08 ± 0.92	5.92 ± 0.67	0.87 ± 0.21
Cu^{2+}-hNF	4.05 ± 0.36	3.20 ± 0.23	2.34 ± 0.17	0.58 ± 0.09
Ca^{2+}-hNF	2.84 ± 0.26	7.50 ± 0.52	5.49 ± 0.38	1.93 ± 0.31

The Michaelis constant K_M value indicates the affinity of the enzyme active sites towards the substrate, in this case, phenol. Smaller values of K_M represent greater affinity. The K_M was 6.82 μmol.mL^{-1} in free enzyme, 4.05 μmol.mL^{-1} in copper hybrids, and 2.84 μmol.mL^{-1} in calcium hybrids. This outcome suggests that both hybrids, especially calcium ones, have more affinity to the substrate than free enzyme, favoring the reaction.

However, despite superior stability in binding enzyme–substrate after immobilization, V_{max} was not increased for either hybrid compared to the free enzyme. In fact, the value did not present considerable change from 8.08 μmol.min^{-1}.mg^{-1} in free enzyme to 7.50 μmol.min^{-1}.mg^{-1} in copper hybrids, although this value decreased to 3.20 μmol.min^{-1}.mg^{-1} in Cu^{2+}-hNF. Correspondingly, magnetic-activated lipase-inorganic hybrid nanoflowers prepared by Zhong et al. (2021) have also presented smaller K_M and V_{max} values than the free enzyme, evidencing a deeper affinity between the enzyme and the substrate does not necessarily induce a higher reaction rate [78].

The turnover number, or k_{cat}, representing the frequency of substrate molecules converted into products by one enzyme molecule, remained similar in calcium hybrids and decreased considerably in copper hybrids compared to the free enzyme. Nevertheless, k_{cat}/K_M value was 2.23 times higher in calcium hybrids than in the free enzyme, indicating that immobilization of free HRP into these hybrids might lead to higher enzymatic efficiency. Zhang et al. (2020) reported similar kinetic results using lipase as an organic portion. The authors have shown that catalytic efficiency was greater for calcium hybrids and smaller for copper. At the same time, K_M was lower for both calcium and copper hybrids than the free enzyme values [19]. A 2.2-fold higher catalytic efficiency than the free enzyme was equally described by Patel et al. (2018), employing copper-laccase nanoflowers cross-linked with glutaraldehyde [17].

Membrane-Based Phenol Biosensing

The membrane-based biosensors, produced onto PVDF hydrophilic membranes with a pore size of 0.22 μm, were tested with 50 μL of a sample, with pH 7.4, containing H_2O_2 0.88 μmol.mL^{-1}, 4-AAP 1.1 μmol.mL^{-1}, and phenol concentrations of 24.00, 19.20, 14.40, 9.60, 4.80, 2.40, 1.44, 0.96, and 0.72 μmol.mL^{-1} (Fig. 14A-J, respectively). Figure 14 shows the biosensors produced with (1) free HRP, (2) Cu^{2+}-hNF, and (3) Ca^{2+}-hNF after 1 min of reaction time at 25 °C. Three measurements were performed for each phenol concentration in all biosensors to confirm the results.

Both biosensors produced with HRP-copper and HRP-calcium hybrids effectively detected phenol ranging from 0.72 to 24.00 μmol.mL^{-1}. Although color change seems greater in calcium hybrids at higher phenol concentrations, as in Fig. 14A, probably due to their higher catalytic efficiency, both calcium and copper biosensors showed similar performance for phenol detection within the concentration range tested. Control biosensors,

produced with an equivalent amount of free enzyme (Fig. 14 (1)), did not present any considerable color switch in none of the phenol concentrations tested. It might have occurred due to enzyme spread through the membrane pores, attenuating visible changes.

It was noticeable in metal-HRP hybrid biosensors that the pink color softened with the decreasing phenol concentration. The smallest concentration of phenol where it was possible to detect the visible color change under the experimental conditions was 0.72 μmol. mL^{-1}. Below this concentration, no color was seen in any biosensors within 1 min.

A colorimetric method for phenol sensing using copper-laccase nanoflowers developed by Zhu et al. (2013) detected phenol in a similar range from 0.4 to 50 μmol.mL^{-1}. However, those results were obtained with a higher reaction time of 5 min [35]. Another phenol biosensing using enzyme-inorganic hybrids was described by Lin et al. (2014). Even though the authors have achieved an excellent detection limit (LOD) of 1.0 μM, the method uses greater sample volume, hybrids amount, and reaction time [42].

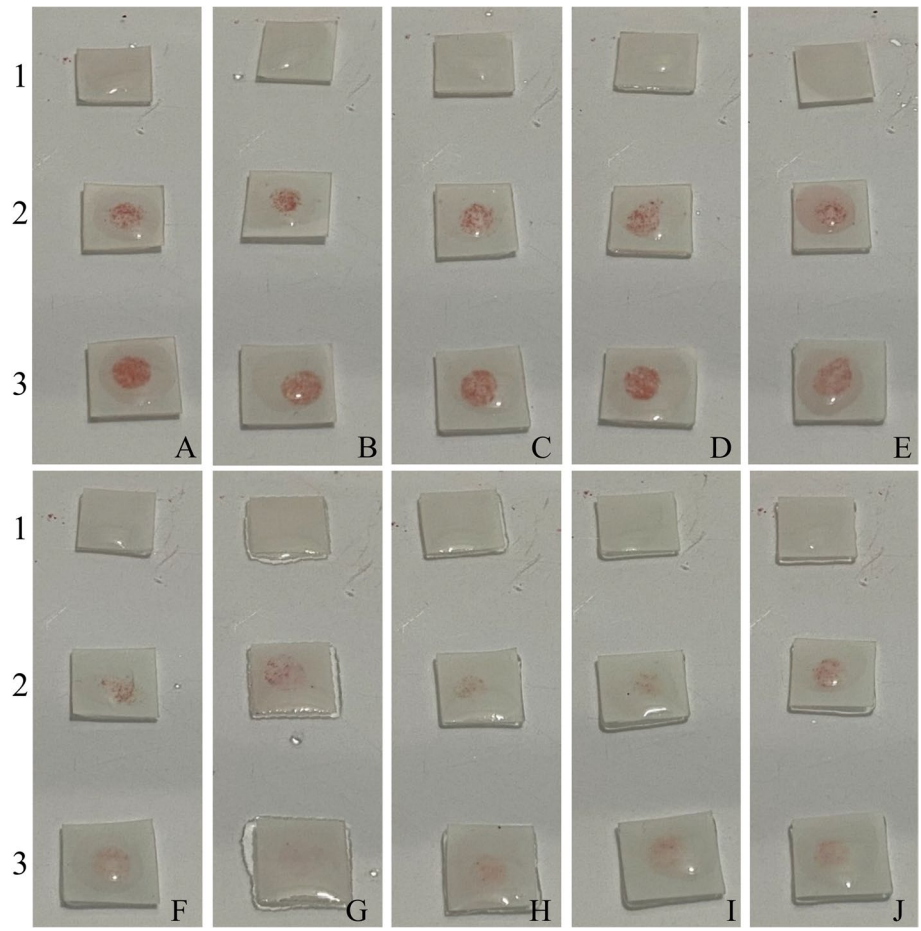

Fig. 14 Images of the biosensors produced with (1) free-HRP, (2) Cu^{2+}-hNF, and (3) Ca^{2+}-hNF after 1 min reaction with different initial concentrations of phenol of (A) 24.00, (B) 19.20, (C) 14.40, (D) 9.60, (E) 4.80, (F) 2.40, (G) 1.92, (H) 1.44, (I) 0.96, and (J) 0.72 μmol.$mL.^{-1}$

A typical synthesis of hybrid nanoflowers following the methodology described in the present work uses only 2.5 mg of HRP and can produce up to 200 units of phenol detection. It might evidence a simple, low-cost, and efficient approach to assembling qualitative enzymatic biosensors for a rapid phenol detection in concentrations up from 0.72 μmol. mL^{-1}. The simplicity of this approach might also represent greater viability for a fast in situ analysis to determine the presence of phenol in the environment.

Conclusion

A simple, rapid, and low-cost, qualitative biosensor for visual detection phenol using copper-HRP and calcium-HRP hybrid nanoflowers were successfully developed. The biosensors prepared with both hybrids could detect phenol in concentrations ranging from 0.72 to 24.00 μmol.mL^{-1} within only 1 min of reaction time. Furthermore, despite the divergence in hybrid morphologies depending on the ion used in their synthesis, Cu^{2+}-hNF and Ca^{2+}-hNF proper formation was confirmed by EDS, FTIR, and XRD analysis. Both hybrids have presented excellent pH and thermal stability, especially calcium ones, maintaining their activity for longer periods in elevated temperatures. In addition, kinetic parameter evaluation has shown a higher catalytic efficiency in Ca^{2+}-hNF than in the free enzyme. Considering all these facts, we believe that the developed biosensor could be a helpful tool in practical and rapid in situ phenol detection.

Acknowledgements The authors would also like to thank LCME – UFSC for the technical support during electron microscopy analysis and Conselho Nacional de Desenvolvimento Científico e Tecnológico (CNPq).

Author Contribution All authors contributed to the study's conception and design. F.P. da Costa: material preparation, data collection, analysis, and original draft. R. O. Henriques: writing, review, and editing. A. Furigo Jr: Project administration.

All authors read and approved the final manuscript.

Funding This study was financed in part by the Coordenação de Aperfeiçoamento de Pessoal de Nível Superior—Brasil (CAPES)—Finance Code 001.

Declarations

Ethics Approval Not applicable.

Consent to Participate Not applicable.

Consent to Publish Not applicable.

Competing Interests The authors declare no competing interests.

References

1. Li, X., Li, S., Liang, X., McClements, D. J., Liu, X., & Liu, F. (2020). Applications of oxidases in modification of food molecules and colloidal systems: Laccase, peroxidase and tyrosinase. *Trends in Food Science and Technology, 103*(March), 78–93.
2. Zhu, Y., Tao, H., Janaswamy, S., Zou, F., Cui, B., & Guo, L. (2021). The functionality of laccase- or peroxidase-treated potato flour: Role of interactions between protein and protein/starch. *Food Chemistry, 341*(February 2020), 128082.

3. BagheriPebdeni, A., & Hosseini, M. (2020). Fast and selective whole cell detection of Staphylococcus aureus bacteria in food samples by paper based colorimetric nanobiosensor using peroxidase-like catalytic activity of DNA-Au/Pt bimetallic nanoclusters. *Microchemical Journal, 159*(September), 105475.
4. Touahar, I. E., Haroune, L., Ba, S., Bellenger, J. P., & Cabana, H. (2014). Characterization of combined cross-linked enzyme aggregates from laccase, versatile peroxidase and glucose oxidase, and their utilization for the elimination of pharmaceuticals. *Science of the Total Environment, 481*, 90–99.
5. Poliakov, A. E., Dumshakova, A. V., Muginova, S. V., & Shekhovtsova, T. N. (2011). A peroxidase-based method for the determination of dopamine, adrenaline, and α-methyldopa in the presence of thyroid hormones in pharmaceutical forms. *Talanta, 84*(3), 710–716.
6. Na, S. Y., & Lee, Y. (2017). Elimination of trace organic contaminants during enhanced wastewater treatment with horseradish peroxidase/hydrogen peroxide (HRP/H2O2) catalytic process. *Catalysis Today, 282*, 86–94.
7. Al-Dhabi, N. A., Esmail, G. A., & Valan Arasu, M. (2021). Effective degradation of tetracycline by manganese peroxidase producing Bacillus velezensis strain Al-Dhabi 140 from Saudi Arabia using fibrous-bed reactor. *Chemosphere, 268*, 128726.
8. Yadav, N., Govindwar, S. P., Rane, N., Ahn, H.-J., Xiong, J.-Q., Jang, M., … Jeon, B.-H. (2021). Insights on the role of periphytic biofilm in synergism with Iris pseudacorus for removing mixture of pharmaceutical contaminants from wastewater.Journal of Hazardous Materials, 418(March), 126349.
9. Garg, S., Kumar, P., Singh, S., Yadav, A., Dumée, L. F., Sharma, R. S., & Mishra, V. (2020). Prosopis juliflora peroxidases for phenol remediation from industrial wastewater — An innovative practice for environmental sustainability. *Environmental Technology and Innovation, 19*, 100865.
10. Darwesh, O. M., Matter, I. A., & Eida, M. F. (2019). Development of peroxidase enzyme immobilized magnetic nanoparticles for bioremediation of textile wastewater dye. *Journal of Environmental Chemical Engineering, 7*(1), 102805.
11. de Oliveira, F. K., Santos, L. O., & Buffon, J. G. (2021). Mechanism of action, sources, and application of peroxidases. *Food Research International, 143*(March), 110266.
12. Sheldon, R. A., & van Pelt, S. (2013). Enzyme immobilisation in biocatalysis: Why, what and how. *Chemical Society reviews, 42*(15), 6223–6235.
13. Ge, J., Lei, J., & Zare, R. N. (2012). Protein-inorganic hybrid nanoflowers. *Nature Nanotechnology, 7*(7), 428–432.
14. Maurya, S. S., Nadar, S. S., & Rathod, V. K. (2020). Dual activity of laccase-lysine hybrid organic–inorganic nanoflowers for dye decolourization. *Environmental Technology and Innovation, 19*, 100798.
15. Wang, S., Ding, Y., Chen, R., Hu, M., Li, S., Zhai, Q., & Jiang, Y. (2018). Multilayer petal-like enzymatic-inorganic hybrid micro-spheres [CPO-(Cu/Co/Cd)3(PO4)2] with high bio-catalytic activity. *Chemical Engineering Research and Design, 134*(620), 52–61.
16. Rong, J., Zhang, T., Qiu, F., & Zhu, Y. (2017). Preparation of Efficient, stable, and reusable laccase-Cu 3 (PO 4) 2 hybrid microspheres based on copper foil for decoloration of Congo red. *ACS Sustainable Chemistry and Engineering, 5*(5), 4468–4477.
17. Patel, S. K. S., Otari, S. V., Li, J., Kim, D. R., Kim, S. C., Cho, B. K., … Lee, J. K. (2018). Synthesis of cross-linked protein-metal hybrid nanoflowers and its application in repeated batch decolorization of synthetic dyes. Journal of Hazardous Materials, 347, 442–450.
18. Wang, A., Chen, X., Yu, J., Li, N., Li, H., Yin, Y., … Wu, S. G. (2020). Green preparation of lipase@ Ca3(PO4)2 hybrid nanoflowers using bone waste from food production for efficient synthesis of clindamycin palmitate. *Journal of Industrial and Engineering Chemistry*, *89*, 383–391.
19. Zhang, Y., Sun, W., Elfeky, N. M., Wang, Y., Zhao, D., Zhou, H., …Bao, Y. (2020). Self-assembly of lipase hybrid nanoflowers with bifunctional Ca2+ for improved activity and stability. Enzyme and Microbial Technology, 132(2), 109408.
20. He, X., Chen, L., He, Q., Xiao, H., Zhou, X., & Ji, H. (2017). Cytochrome P450 enzyme-copper phosphate hybrid nano-flowers with superior catalytic performances for selective oxidation of sulfides. *Chinese Journal of Chemistry, 35*(5), 693–698.
21. Li, W. Y., Lu, S. Y., Bao, S. J., Shi, Z. Z., Lu, Z., Li, C. M., & Yu, L. (2018). Efficient in situ growth of enzyme-inorganic hybrids on paper strips for the visual detection of glucose. *Biosensors and Bioelectronics, 99*(August 2017), 603–611.
22. Cheon, H. J., Adhikari, M. D., Chung, M., Tran, T. D., Kim, J., & Kim, M. I. (2019). Magnetic nanoparticles-embedded enzyme-inorganic hybrid nanoflowers with enhanced peroxidase-like activity and substrate channeling for glucose biosensing. *Advanced Healthcare Materials, 8*(9), 1–8.
23. Batule, B. S., Park, K. S., Gautam, S., Cheon, H. J., Kim, M. I., & Park, H. G. (2019). Intrinsic peroxidase-like activity of sonochemically synthesized protein copper nanoflowers and its application for the sensitive detection of glucose. *Sensors and Actuators, B: Chemical, 283*(June 2018), 749–754.

24. Zhang, M., Yang, N., Liu, Y., & Tang, J. (2019). Synthesis of catalase-inorganic hybrid nanoflowers via sonication for colorimetric detection of hydrogen peroxide. *Enzyme and Microbial Technology, 128*(March), 22–25.
25. Altinkaynak, C., Yilmaz, I., Koksal, Z., Özdemir, H., Ocsoy, I., & Özdemir, N. (2016). Preparation of lactoperoxidase incorporated hybrid nanoflower and its excellent activity and stability. *International Journal of Biological Macromolecules, 84*, 402–409.
26. Ye, R., Zhu, C., Song, Y., Song, J., Fu, S., Lu, Q., … Lin, Y. (2016). One-pot bioinspired synthesis of all-inclusive protein-protein nanoflowers for point-of-care bioassay: Detection of: E. coli O157:H7 from milk. *Nanoscale*, *8*(45), 18980–18986.
27. Gay, N. H., Phopin, K., Suwanjang, W., Songtawee, N., Ruankham, W., Wongchitrat, P., & Prachayasittikul, V. (2018). Neuroprotective effects of phenolic and carboxylic acids on oxidative stress-induced toxicity in human neuroblastoma SH-SY5Y cells. *Neurochemical Research, 43*(3), 619–636.
28. Jun, L. Y., Yon, L. S., Mubarak, N. M., Bing, C. H., Pan, S., Danquah, M. K., & Khalid, M. (2019). An overview of immobilized enzyme technologies for dye and phenolic removal from wastewater. *Journal of Environmental Chemical Engineering, 7*(2):102961
29. Arciuli, M., Palazzo, G., Gallone, A., & Mallardi, A. (2013). Bioactive paper platform for colorimetric phenols detection. *Sensors and Actuators, B: Chemical, 186*, 557–562.
30. Guan, Y., Liu, L., Chen, C., Kang, X., & Xie, Q. (2016). Effective immobilization of tyrosinase via enzyme catalytic polymerization of L-DOPA for highly sensitive phenol and atrazine sensing. *Talanta, 160*, 125–132.
31. Abdullah, J., Ahmad, M., Karuppiah, N., Heng, L. Y., & Sidek, H. (2006). Immobilization of tyrosinase in chitosan film for an optical detection of phenol. *Sensors and Actuators, B: Chemical, 114*(2), 604–609.
32. Hashim, H. S., Fen, Y. W., Sheh Omar, N. A., Abdullah, J., Daniyal, W. M. E. M. M., & Saleviter, S. (2020). Detection of phenol by incorporation of gold modified-enzyme based graphene oxide thin film with surface plasmon resonance technique. *Optics Express, 28*(7), 9738.
33. Wen, Y., Li, R., Liu, J., Zhang, X., Wang, P., Zhang, X., & Sun, B. (2020). Promotion effect of Zn on 2D bimetallic NiZn metal organic framework nanosheets for tyrosinase immobilization and ultrasensitive detection of phenol. *Analytica Chimica Acta, 1127*, 131–139.
34. Zhang, S., Zhao, H., & John, R. (2001). A dual-phase biosensing system for the determination of phenols in both aqueous and organic media. *Analytica Chimica Acta, 441*(1), 95–105.
35. Zhu, L., Gong, L., Zhang, Y., Wang, R., Ge, J., Liu, Z., & Zare, R. N. (2013). Rapid detection of phenol using a membrane containing laccase nanoflowers. *Chemistry - An Asian Journal, 8*(10), 2358–2360.
36. Casero, E., Petit-Domínguez, M. D., Vázquez, L., Ramírez-Asperilla, I., Parra-Alfambra, A. M., Pariente, F., & Lorenzo, E. (2013). Laccase biosensors based on different enzyme immobilization strategies for phenolic compounds determination. *Talanta, 115*, 401–408.
37. Roy, J. J., Abraham, T. E., Abhijith, K. S., Kumar, P. V. S., & Thakur, M. S. (2005). Biosensor for the determination of phenols based on Cross-Linked Enzyme Crystals (CLEC) of laccase. *Biosensors and Bioelectronics, 21*(1), 206–211.
38. Othman, A. M., & Wollenberger, U. (2020). Amperometric biosensor based on coupling aminated laccase to functionalized carbon nanotubes for phenolics detection. *International Journal of Biological Macromolecules, 153*, 855–864.
39. Jarosz-Wilkołazka, A., Ruzgas, T., & Gorton, L. (2005). Amperometric detection of mono- and diphenols at Cerrena unicolor laccase-modified graphite electrode: Correlation between sensitivity and substrate structure. *Talanta, 66*(5), 1219–1224.
40. Cho, S. H., Shim, J., Yun, S. H., & Moon, S. H. (2008). Enzyme-catalyzed conversion of phenol by using immobilized horseradish peroxidase (HRP) in a membraneless electrochemical reactor. *Applied Catalysis A: General, 337*(1), 66–72.
41. Rosatto, S. S., Sotomayor, P. T., Kubota, L. T., & Gushikem, Y. (2002). SiO2/Nb2O5 sol-gel as a support for HRP immobilization in biosensor preparation for phenol detection. *Electrochimica Acta, 47*(28), 4451–4458.
42. Lin, Z., Xiao, Y., Yin, Y., Hu, W., Liu, W., & Yang, H. (2014). Facile synthesis of enzyme-inorganic hybrid nanoflowers and its application as a colorimetric platform for visual detection of hydrogen peroxide and phenol. *ACS Applied Materials and Interfaces, 6*(13), 10775–10782.
43. Ozoner, S. K., Keskinler, B., & Erhan, E. (2011). HRP immobilized microporous Poly(styrene-divinylbenzene-polyglutaraldehyde) monolith for forced flow injected phenol biosensing. *Materials Science and Engineering C, 31*(3), 663–668.

44. Rahemi, V., Trashin, S., Hafideddine, Z., Meynen, V., Van Doorslaer, S., & De Wael, K. (2019). Enzymatic sensor for phenols based on titanium dioxide generating surface confined ROS after treatment with H2O2. *Sensors and Actuators, B: Chemical, 283*(December 2018), 343–348.
45. Çevik, E., Şenel, M., Baykal, A., & Abasiyanik, M. F. (2012). A novel amperometric phenol biosensor based on immobilized HRP on poly(glycidylmethacrylate)-grafted iron oxide nanoparticles for the determination of phenol derivatives. *Sensors and Actuators, B: Chemical, 173*, 396–405.
46. Yang, S., Chen, Z., Jin, X., & Lin, X. (2006). HRP biosensor based on sugar-lectin biospecific interactions for the determination of phenolic compounds. *Electrochimica Acta, 52*(1), 200–205.
47. Nadar, S. S., Gawas, S. D., & Rathod, V. K. (2016). Self-assembled organic–inorganic hybrid glucoamylase nanoflowers with enhanced activity and stability. *International Journal of Biological Macromolecules, 92*, 660–669.
48. Altinkaynak, C., Gulmez, C., Atakisi, O., & Özdemir, N. (2020). Evaluation of organic-inorganic hybrid nanoflower's enzymatic activity in the presence of different metal ions and organic solvents. *International Journal of Biological Macromolecules, 164*, 162–171.
49. Talens-Perales, D., Fabra, M. J., Martínez-Argente, L., Marín-Navarro, J., & Polaina, J. (2020). Recyclable thermophilic hybrid protein-inorganic nanoflowers for the hydrolysis of milk lactose. *International Journal of Biological Macromolecules, 151*, 602–608.
50. Ghosh, K., Balog, E. R. M., Sista, P., Williams, D. J., Kelly, D., Martinez, J. S., & Rocha, R. C. (2014). Temperature-dependent morphology of hybrid nanoflowers from elastin-like polypeptides. *APL Materials, 2*(021101), 1–6
51. Trinder, P. (1969). Determination of glucose in blood using glucose oxidase with an alternative oxygen acceptor. *Annals of Clinical Biochemistry: International Journal of Laboratory Medicine, 6*(1), 24–27.
52. Malmstadt, H., & Hadjiioannou, T. (1963). Specific enzymatic determination of some alpha-amino acids by an automatic spectrophotometric reaction rate method. *Analytical Chemistry, 35*(1), 4–16.
53. Sun, J., Ge, J., Liu, W., Lan, M., Zhang, H., Wang, P., & Niu, Z. (2014). Multi-enzyme co-embedded organic-inorganic hybrid nanoflowers: Synthesis and application as a colorimetric sensor. *Nanoscale, 6*(1), 255–262.
54. Memon, A. H., Ding, R., Yuan, Q., Wei, Y., & Liang, H. (2019). Facile synthesis of alcalase-inorganic hybrid nanoflowers used for soy protein isolate hydrolysis to improve its functional properties. *Food Chemistry, 289*, 568–574.
55. Somturk, B., Yilmaz, I., Altinkaynak, C., Karatepe, A., Özdemir, N., & Ocsoy, I. (2016). Synthesis of urease hybrid nanoflowers and their enhanced catalytic properties. *Enzyme and Microbial Technology, 86*, 134–142.
56. Aydemir, D., Gecili, F., Özdemir, N., & Nuray Ulusu, N. (2020). Synthesis and characterization of a triple enzyme-inorganic hybrid nanoflower (TrpE@ihNF) as a combination of three pancreatic digestive enzymes amylase, protease and lipase. *Journal of Bioscience and Bioengineering, 129*(6), 679–686.
57. Jiang, W., Wang, X., Yang, J., Han, H., Li, Q., & Tang, J. (2018). Lipase-inorganic hybrid nanoflower constructed through biomimetic mineralization: A new support for biodiesel synthesis. *Journal of Colloid and Interface Science, 514*, 102–107.
58. Li, Y., Fei, X., Liang, L., Tian, J., Xu, L., Wang, X., & Wang, Y. (2016). The influence of synthesis conditions on enzymatic activity of enzyme-inorganic hybrid nanoflowers. *Journal of Molecular Catalysis B: Enzymatic, 133*, 92–97.
59. Yu, J., Wang, C., Wang, A., Li, N., Chen, X., Pei, X., … Wu, S. G. (2018). Dual-cycle immobilization to reuse both enzyme and support by reblossoming enzyme-inorganic hybrid nanoflowers. *RSC Advances*, *8*(29), 16088–16094.
60. Ke, C., Fan, Y., Chen, Y., Xu, L., & Yan, Y. (2016). A new lipase-inorganic hybrid nanoflower with enhanced enzyme activity. *RSC Advances, 6*(23), 19413–19416.
61. Chung, M., Nguyen, T. L., Tran, T. Q. N., Yoon, H. H., Kim, I. T., & Kim, M. I. (2018). Ultrarapid sonochemical synthesis of enzyme-incorporated copper nanoflowers and their application to mediatorless glucose biofuel cell. *Applied Surface Science, 429*, 203–209.
62. Batule, B. S., Park, K. S., Kim, M. I., & Park, H. G. (2015). Ultrafast sonochemical synthesis of protein-inorganic nanoflowers. *International Journal of Nanomedicine, 10*, 137–142.
63. Gulmez, C., Altinkaynak, C., Özdemir, N., & Atakisi, O. (2018). Proteinase K hybrid nanoflowers (P-hNFs) as a novel nanobiocatalytic detergent additive. *International Journal of Biological Macromolecules, 119*, 803–810.
64. Koca, F. D., Demirezen Yilmaz, D., Ertas Onmaz, N., & Ocsoy, I. (2020). Peroxidase-like activity and antimicrobial properties of curcumin-inorganic hybrid nanostructure. *Saudi Journal of Biological Sciences, 27*(10), 2574–2579.

65. Ren, W., Li, Y., Wang, J., Li, L., Xu, L., Wu, Y., … Tian, J. (2019). Synthesis of magnetic nanoflower immobilized lipase and its continuous catalytic application. *New Journal of Chemistry*, *43*(28), 11082–11090.
66. Ariza-Avidad, M., Salinas-Castillo, A., & Capitán-Vallvey, L. F. (2016). A 3D μPAD based on a multienzyme organic-inorganic hybrid nanoflower reactor. *Biosensors and Bioelectronics, 77*, 51–55.
67. He, G., Hu, W., & Li, C. M. (2015). Spontaneous interfacial reaction between metallic copper and PBS to form cupric phosphate nanoflower and its enzyme hybrid with enhanced activity. *Colloids and Surfaces B: Biointerfaces, 135*, 613–618.
68. Altinkaynak, C., Tavlasoglu, S., Kalin, R., Sadeghian, N., Ozdemir, H., Ocsoy, I., & Özdemir, N. (2017). A hierarchical assembly of flower-like hybrid Turkish black radish peroxidase-Cu2+ nanobiocatalyst and its effective use in dye decolorization. *Chemosphere, 182*, 122–128.
69. Alessi, A., Agnello, S., Buscarino, G., & Gelardi, F. M. (2013). Raman and IR investigation of silica nanoparticles structure. *Journal of Non-Crystalline Solids, 362*(1), 20–24.
70. Yu, Y., Fei, X., Tian, J., Xu, L., Wang, X., & Wang, Y. (2015). Self-assembled enzyme-inorganic hybrid nanoflowers and their application to enzyme purification. *Colloids and Surfaces B: Biointerfaces, 130*, 299–304.
71. Sun, X., Niu, H., Song, J., Jiang, D., Leng, J., Zhuang, W., … Ying, H. (2020). Preparation of a copper polyphosphate kinase hybrid nanoflower and its application in ADP regeneration from AMP. *ACS Omega*, *5*(17), 9991–9998.
72. Cui, J., Zhao, Y., Liu, R., Zhong, C., & Jia, S. (2016). Surfactant-activated lipase hybrid nanoflowers with enhanced enzymatic performance. *Scientific Reports, 6*(29), 1–13.
73. Hao, M., Fan, G., Zhang, Y., Xin, Y., & Zhang, L. (2019). Preparation and characterization of copper-Brevibacterium cholesterol oxidase hybrid nanoflowers. *International Journal of Biological Macromolecules, 126*, 539–548.
74. Cheng, P., Tang, M., Chen, Z., Liu, W., Jiang, X., Pei, X., & Su, W. (2020). Dual-enzyme and NADPH co-embedded organic-inorganic hybrid nanoflowers prepared using biomimetic mineralization for the asymmetric synthesis of (: R)-(-)-pantolactone. *Reaction Chemistry and Engineering, 5*(10), 1973–1980.
75. Chen, X., Xu, L., Wang, A., Li, H., Wang, C., Pei, X., … Wu, S. G. (2018). Efficient synthesis of the key chiral alcohol intermediate of Crizotinib using dual-enzyme@CaHPO4 hybrid nanoflowers assembled by mimetic biomineralization.*Journal of Chemical Technology and Biotechnology*, *94*(1), 236–243.
76. Duan, L., Li, H., & Zhang, Y. (2018). Synthesis of hybrid nanoflower-based carbonic anhydrase for enhanced biocatalytic activity and stability. *ACS Omega, 3*(12), 18234–18241.
77. Metelitza, D. I., Litvinchuk, A. V., & Savenkova, M. I. (1991). Peroxidase-catalyzed co-oxidation of halogen-substituted phenols and 4-aminoantipyrine. *Journal of Molecular Catalysis, 67*(3), 401–411.
78. Zhong, L., Jiao, X., Hu, H., Shen, X., Zhao, J., Feng, Y., … Jia, S. (2021). Activated magnetic lipase-inorganic hybrid nanoflowers: A highly active and recyclable nanobiocatalyst for biodiesel production. *Renewable Energy*, *171*, 825–832.